Articles

Structure−Activity Relationships and Pharmacokinetic Analysis for a Series of Potent, Systemically Available Biphenylsulfonamide Matrix Metalloproteinase Inhibitors

Patrick M. O'Brien,* Daniel F. Ortwine, Alexander G. Pavlovsky, Joseph A. Picard, Drago R. Sliskovic, Bruce D. Roth, Richard D. Dyer,[†] Linda L. Johnson,[†] Chiu Fai Man,[†] and Hussein Hallak[‡]

Departments of Chemistry, Biochemistry, and Pharmacokinetics/Drug Metabolism, Parke-Davis Pharmaceutical Research, Division of Warner Lambert Company, 2800 Plymouth Road, Ann Arbor, Michigan 48105

A series of biphenylsulfonamide derivatives of (*S*)-2-(biphenyl-4-sulfonylamino)-3-methylbutyric acid (**5**) were prepared and evaluated for their ability to inhibit matrix metalloproteinases (MMPs). For this series of compounds, our objective was to systematically replace substituents appended to the biphenyl and α-position of **5** with structurally diverse functionalities to assess the effects these changes have on biological and pharmacokinetic activity. The ensuing structure−activity relationship (SAR) studies showed that biphenylsulfonamides substituted with bromine in the 4′-position (**11c**) significantly improved in vitro activity and exhibited superior pharmacokinetics (C_{max}, $t_{1/2}$, AUCs), relative to compound **5**. Varying the lipophilicity of the α-position by replacing the isopropyl group of **11c** with a variety of substituents, in general, maintained potency versus MMP-2, -3, and -13 but decreased the oral systemic availability. Subsequent evaluation of its enantiomer, **11c′**, showed that both compounds were equally effective MMP inhibitors. In contrast, the corresponding hydroxamic acid enantiomeric pair, **16a** (*S*-isomer) and **16a′** (*R*-isomer), stereoselectivity inhibited MMPs. For the first time in this series, **16a′** provided nanomolar potency against MMP-1, -7, and -9 (IC$_{50}$'s = 110, 140, and 18 nM, respectively), whereas **16a** was less potent against these MMPs (IC$_{50}$'s = 24, 78, and 84 μM, respectively). However, unlike **11c**, compound **16a′** afforded very low plasma concentrations following a single 5 mg/kg oral dose in rat. Subsequent X-ray crystal structures of the catalytic domain of stromelysin (MMP-3CD) complexed with inhibitors from closely related series established the differences in the binding mode of carboxylic acid-based inhibitors (**11c,c′**) relative to the corresponding hydroxamic acids (**16a,a′**).

Introduction

Matrix metalloproteinases (MMPs) are a family of zinc-dependent, calcium-containing endopeptidases that have been shown to play a significant physiological role in tissue remodeling in normal growth and development.[1] Regulation of their proteolytic activity in tissue remodeling is controlled by a variety of mechanisms, including inhibition by endogenous tissue inhibitors of metalloproteinases (TIMPS).[2] An imbalance in the MMP/TIMP ratio favoring the overproduction of MMPs has been implicated in a number of pathological processes, including the destruction of cartilage and bone in rheumatoid arthritis and osteoarthritis, tumor growth and metastasis in both human and animal cancers, degeneration of the aortic wall in abdominal aortic aneurysms, and progressive cardiac dilation in patients with congestive heart failure.[3−6] The accumulation of evidence suggesting that upregulation of MMPs is involved in these, and other disease states, has led to a

growing number of pharmaceutical companies attempting to design and develop orally active inhibitors that may restore the balance of MMP regulation in these pathological processes.

The majority of the MMPs are divided into four main groups that include collagenases (MMP-1, -8, -13), gelatinases (MMP-2, -9), stromelysins (MMP-3, -10, -1) and membrane-type MMPs (MMP-14, -15, -16, -17), while matrilysin (MMP-7) and metalloelastase (MMP-12) are included separately as members of the metalloproteinase family.[7] The primary structures for most of the human MMPs have been determined, demonstrating that each possesses similar structural domains, which include an *N*-terminal propeptide region, a zinc-containing catalytic domain, and, with the exception of matrilysin, a C-terminal domain.[8a] A number of X-ray and NMR structures of MMP catalytic domain/inhibitor complexes have now been reported and show that inhibitor interactions at the active-site zinc play a critical role in defining the binding mode and relative inhibitor potency.[9] Thus, the majority of MMP inhibitors reported in the literature,[10] including those reported to be in clinical trials (Figure 1), contain an effective zinc

* To whom correspondence should be addressed. Tel: 734-622-7076. Fax: 734-622-3107. E-mail: patrick.obrienp@aa.wl.co.
† Department of Biochemistry.
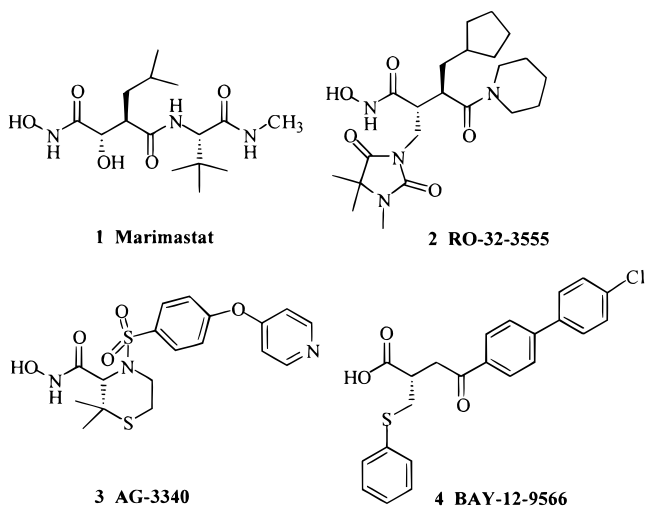‡ Department of Pharmacokinetics/Drug Metabolism.

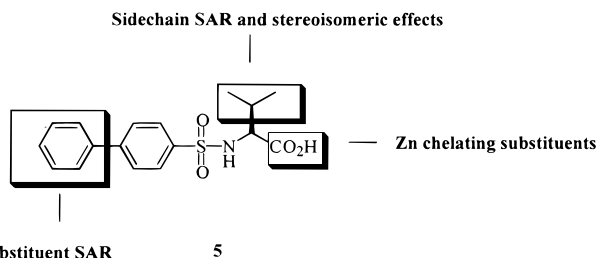**Figure 1.** MMP inhibitors reported to be evaluated in clinical trials.

Figure 2. Proposed biphenylsulfonamide SAR studies.

binding group (e.g. hydroxamic acid, carboxylic acid, sulfhydryl group) that is either generally substituted with a peptide-like structure that mimics the substrates that they cleave or appended to smaller side chains that may interact with specific subsites (e.g, P1′, P2′, P3′) within the active site.[10,11]

To further assess the role of MMPs in vivo, our goal was to identify an inhibitor possessing a suitable pharmacokinetic profile for chronic oral dosing in animal models of arthritis, atherosclerosis, heart failure, and multiple sclerosis. As part of our search for novel MMP inhibitors, we screened our library of compounds and identified (*S*)-2-benzenesulfonylamino-4-methyl-pentanoic acid and 4-biphenyl-4-yl-4-oxobutyric acid (Fenbufen) as selective inhibitors of human MMP-2 and -3 (micromolar potency), having no inhibitory activity against MMP-1, -7, and -9. Replacement of the benzene group of the sulfonamide with Fenbufen's biphenyl led to the identification compound **5** (Figure 2), a biphenyl-sulfonamide derivative that, unlike the benzenesulfona-mides or Fenbufen derivatives, exhibited nanomolar potency vs MMP-2, -3, and -13 and micromolar potency vs MMP-1, -7, and -9. In contrast to our results, Shionogi Research Laboratories reported nanomolar potency vs MMP-9 for a closely related series of *N*-sulfonylamino acid derivatives, several of which exhibited oral activity in animal models of tumor growth and metastasis.[12]

As a tool to complement the in vitro screening, we examined the possible binding modes of **5** with the catalytic domain of MMP-3 through molecular modeling methods based on an X-ray structure previously described.[13] From this study, we found that the major interactions contributing to the tight binding of **5** with MMP-3CD include catalytic zinc−carboxylate coordina-

Scheme 1[a]

R₂ = *t*-Bu **10a,b, g, h, j-l**
R₂ = H **11a,b, g, h, j-l**
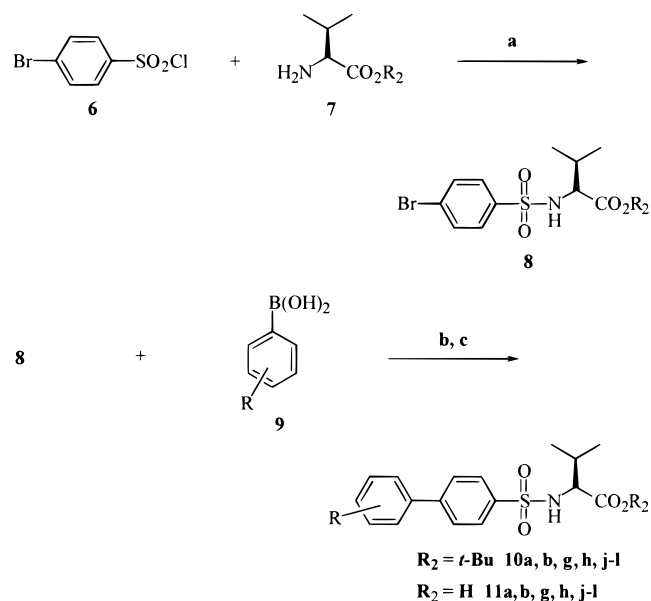
[a] (a) NEt₃, THF/H₂O; (b) Pd(PPh₃)₄, Na₂CO₃, H₂O/ toluene, reflux; (c) anisole, TFA, 25 °C.

tion, hydrogen bonding between the sulfonamide moiety and protein amino acid residues, and hydrophobic interactions plus aromatic stacking of the biphenyl ring system within the P1′ pocket. On the basis of these results, we examined structure−activity relationships (SARs) based on **5**, assessing the effects that structural changes made to the biphenyl ring system, the α-position, and the carboxylate moiety have on biological activity. In this paper, we describe the synthesis, structural analysis, SARs, and pharmacokinetics for analogues of compound **5** and the events leading to the selection of **11c** as a candidate for evaluation in pre-clinical efficacy models.

Chemistry

The synthesis of carboxylic acid derivatives **11a,b**, **g,h,j−l** (Tables 1 and 2) is presented in Scheme 1 (method A). Commercially available 4-bromobenzene-sulfonyl chloride (**6**) was coupled to L-valine *tert*-butyl ester (**7**) in the presence of triethylamine to give the bromobenzenesulfonamide intermediate **8**. Utilizing reaction conditions developed by Suzuki, compound **8** was coupled with a variety of substituted benzenebo-ronic acids **9** via palladium catalysis in refluxing toluene to yield substituted biphenylsulfonamide derivatives **10a,b,g,h,j−l**.[14] Hydrolysis of the *tert*-butyl ester using trifluoroacetic acid in the presence of anisole gave the corresponding carboxylic acid derivatives **11a,b,g,h,j−l**.

Alternatively, biphenylsufonamide carboxylic acids **11c−f,i,m−v** (Tables 1, 2, 4, and 5) were prepared from appropriately substituted biphenyl starting materials **12** as shown in Scheme 2 (method B). Commercially available substituted biphenyls **12** were reacted with chlorosulfonic acid in chloroform to give the biphenyl-sulfonic acids **13**, which were converted to the corre-sponding sulfonyl chlorides **14** in refluxing thionyl chloride. Analogues of **14** were coupled with a variety of amino acid esters **15** in aqueous tetrahydrofuran to yield compounds **10c−f,m,p,q** as *tert*-butyl esters and

Scheme 2[a]

$R_2 = t$-Bu, **10c-f, i, m,p-q**

$R_2 = CH_3$, **10n-o, r-y**

$R_2 = H$, **11c-f, i, m-y**
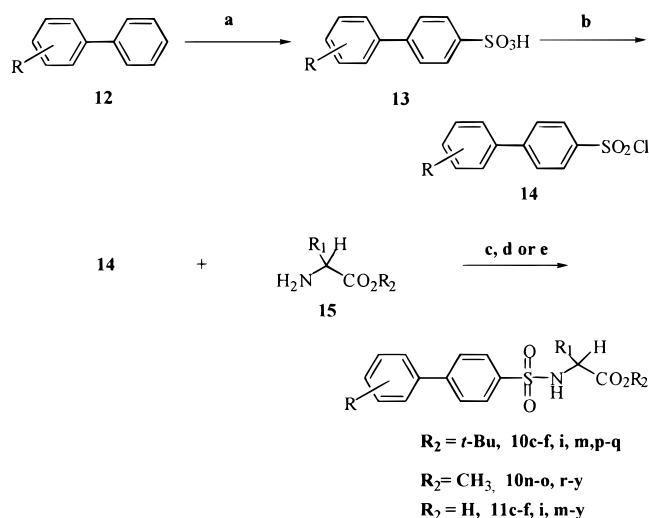
[a] (a) ClSO$_3$H, CHCl$_3$, 25 °C; (b) SOCl$_2$, reflux; (c) NEt$_3$, THF/H$_2$O; (d) anisole, TFA, 25 °C; (e) LiOH, H$_2$O, *p*-dioxane.

Scheme 3[a]
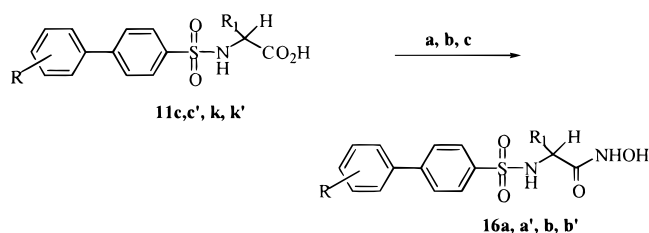
[a] (a) Oxalyl chloride, CH$_2$Cl$_2$, 25 °C; (b) NH$_2$OTHP, NEt$_3$, THF/H$_2$O; (c) HCl.

10n,o,r−v as the corresponding methyl esters. Esters **10c−f,m,p,q** required trifluoroacetic acid hydrolysis to the corresponding acids as previously described, whereas methyl esters **10n,o,r−v** were saponified to the carboxylic acids **11n,o,r−v** using lithium hydroxide in aqueous tetrahydrofuran.

The hydroxamic acid analogues presented in Table 5 (**16a,a′,b,b′**) were synthesized as shown in Scheme 3 (method C). The carboxylic acids **11c,c′,k,k′** were reacted with oxalyl chloride in dichloromethane and coupled with *O*-tetrahydro-2*H*-pyran-2-hydroxylamine to give the protected hydroxamic acids. Acidic hydrolysis of the protecting group gave pure hydroxamic acids (**16a,a′,b,b′**).

Biological Evaluation

All compounds were tested in vitro against a panel of six matrix metalloproteinases, MMP-1, -2, -3, -7, -9, and -13; see the Experimental Section for details on the protocols used. Assays used the catalytic domains of the proteins, with the exceptioon of MMP-1 and -9, where the full-length forms were employed. Results are shown in Tables 1, 2, 4, and 6 for different classes of compounds.
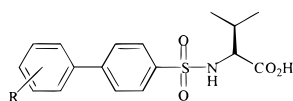
All testing was performed at pH 7, except for MMP-3, where a pH of 6 was used. Among MMPs, MMP-3 exhibits a unique acidic pH optimum of 5.5−6.5 for activity,[15−17] which is due to the presence of a protonated histidine (residue 224) in the S1′ site (see Figure 3).[16,18,19] This histidine is specific to MMP-3 and allowed this protein to be identified as the 'acid metalloprotein-ase' among the family.[15] Mutation of this residue to a nonionizable residue (Gln) resulted in catalytically active protein with a broad pH optimum similar to that of other MMPs.[17,18] Testing at MMP-3's pH optimum allowed us to better differentiate potent inhibitors of this enzyme and to more accurately determine which compounds might be selective for MMP-3.
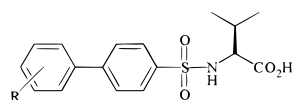
Results and Discussion

Initial SAR studies based on **5** were designed to examine the interaction of the biphenyl ring with the P1′ specificity site within the MMPs of interest. As can be seen from Table 1, **5** exhibits selectivity for MMP-2, -3, and -13 over MMP-1, -7, and -9. Consistent with the in vitro profile for **5**, the S1′ channels of MMP-1 and -7 have been reported to be occluded by arginine and tyrosine residues, respectively, and would therefore have difficulty accommodating the distal phenyl ring of **5**.[13,20] Homology models of MMP-9 suggest an arginine may also play a role in reducing the size of the S1′ channel and therefore reducing the potency of the inhibitor.[21] However, it appears that if enough binding energy is gained from the zinc ligating and sulfonamide portions of the molecule, a reorganization of residues in the channel may occur to allow binding of large S1′ groups with less of a reduction in potency than might be expected.[22] With this in mind, we prepared analogues of **5** substituting the distal phenyl ring of the biphenyl with various halogens (**11a−f**), electron-withdrawing groups (**11j−m**), and electron-donating groups (**11g−i**) (Tables 1 and 2), utilizing the synthetic routes shown in Schemes 1 and 2, and assessed the effects that these changes have on MMP inhibitory activity.

As can be seen in Table 1, halogens appended to the 4′-position of the biphenyl ring (**11a,c,e**), in general, increased potency against MMP-2, -3, -7, and -13 relative to **5**. This magnitude of the increase did not change as the size of the halo substituent was increased from F to Cl to Br. However, substitution at the 3′-position resulted in a decrease in inhibitory activity, particularly for MMPs with narrow or shallow S1′ channels (MMP-1, -7, and -9, respectively), when compared to the corresponding 4′-isomers (compare **11a** vs **11b** and **11c** vs **11d**). Incorporation of a fluorine atom in the 2′-position in **11c** (**11f**) was tolerated and provided a modest increase in potency against MMP-1, -7, and -9 and comparable in vitro activity vs MMP-2 and -3. Electron-withdrawing groups (**11j−m,** Table 2) and moderate electron-donating groups (**11g,h**) significantly improved inhibitory activity against MMP -2, -3, and -13 relative to the unsubstituted biphenyl derivative **5**, while a strongly electron-donating substituent (**11i**) did not. To help understand the observed SAR and to rationalize the specificity profile, we examined the interaction of compound **11c** with the active site of MMP-3CD. Since suitable crystals of an MMP-3CD/complex of compound **11c** could not be obtained for X-ray studies, we modeled **11c** into the protein using coordinates from recently published crystal structures of MMP-3CD complexed with a series of related diphe-nylpiperidine derivatives.[13] In this model (Figures 3 and 4), the 4′-bromobiphenyl moiety resides in the S1′ specificity site, which allows for large substituents in the 4′-position, but not in the 2′- or 3′-position where

Table 1. In Vitro Activity of Halogenated Biphenylsulfonamide Derivatives

					MMPs IC$_{50}$ (μM)[b]					
compd	R	formula[a]	mp (°C)	method	1[c]	2	3[d]	7	9[c]	13
5	H	C$_{17}$H$_{19}$NO$_4$S	164−166	B	5.4	0.040	0.038	71	26	0.062
11a	4-F	C$_{17}$H$_{18}$FNO$_4$S[e]	165−166	A	4.2	0.039	0.010	4.8	64	0.043
11b	4-F	C$_{17}$H$_{18}$FNO$_4$S	145−147	A	8.6	0.049	0.017	22	65	0.150
11c	4-Br	C$_{17}$H$_{18}$BrNO$_4$S	192−193	B	6.0	0.004	0.007	7.2	7.9	0.008
11d	3-Br	C$_{17}$H$_{18}$BrNO$_4$S	foam	B	100	0.535	0.290	100	100	0.710
11e	4-Cl	C$_{17}$H$_{18}$ClNO$_4$S	187−188	B	6.5	0.011	0.009	7.5	16	0.048
11f	2-F,4-Br	C$_{17}$H$_{17}$BrFINO$_4$S	175−177	B	3.6	0.005	0.016	2.1	4.9	0.007

[a] Analytical results are within ±0.4% of the theoretical values unless otherwise noted. [b] MMP inhibition in vitro. Except where noted, assays were run at pH 7 against the catalytic domains of the enzymes. See the Experimental Section for complete protocols. [c] Full-length version of the enzyme was used. [d] Assay was run at pH 6. Unlike other MMPs, MMP-3 displays a strong pH dependence and is maximally active at pH 5.5−6.[15−17] See the Biological Evaluation and Experimental Section for details. [e] Anal. C: calcd 58.11, found 57.66; H: calcd 5.16, found 5.18; N: calcd 3.99, found 3.69.

Table 2. In Vitro Activity of Biphenylsulfonamide Derivatives Substituted with Electron-Donating or Electron-Withdrawing Functionalities

					MMPs IC$_{50}$ (μM)[b]					
compd	R	formula[a]	mp (°C)	method	1[c]	2	3[d]	7	9[c]	13
5	H	C$_{17}$H$_{19}$NO$_4$S	164−166	B	5.4	0.040	0.038	71	26	0.062
11g	4-CH$_3$	C$_{18}$H$_{21}$NO$_4$S	185−186	A	2.2	0.002	0.003	4.5	3.9	0.011
11h	4-OCH$_3$	C$_{18}$H$_{21}$NO$_5$S	180−181	A	1.5	0.003	0.008	7.2	2.2	0.006
11i	4-NH$_2$	C$_{17}$H$_{20}$N$_2$O$_4$S[e]	>230	B	26	0.036	0.036	31	20	0.105
11j	4-CF$_3$	C$_{18}$H$_{18}$F$_3$NO$_4$S	183−184	A	4.2	0.013	0.009	7.9	20	0.023
11k	4-CN	C$_{18}$H$_{18}$N$_2$O$_4$S	182−183	A	18	0.033	0.006	7.0	59	0.037
11l	4-CHO	C$_{18}$H$_{19}$NO$_5$S	189−190	A	3.2	0.012	0.008	4.5	17	0.016
11m	4-NO$_2$	C$_{17}$H$_{18}$N$_2$O$_6$S	167−169	B	12	0.061	0.015	5.6	38	0.102

[a−d] Refer to footnotes in Table 1. [e] Anal. C: calcd 58.60, found 58.42; H: calcd 5.79, found 5.23; N: calcd 8.04, found 7.65.

the channel narrows. Major interactions contributing to the tight binding of **11c** include carboxylic acid−zinc ligation, the carboxylate hydrogen bonding with Glu 202, and hydrogen bonding between the sulfonamide moiety and Ala 165 and Leu 164. In addition, substitution by electron-withdrawing substituents produces an electron-deficient phenyl ring, which in turn can improve aryl−aryl stacking interactions with His 201 (sandwich stack; distance between ring centroids = 3.5 Å) and Tyr 223 (edge-to-face interaction; average distance between His ring centroid and the two proximal Tyr ring carbons = 4.6 Å) in the active site. The reduction in binding energy resulting from a reduced $\pi-\pi$ stack by phenyl rings para-substituted by moderate electron-releasing groups (CH$_3$, OCH$_3$) appears to be more than offset by the increase in steric bulk/lipophilic contacts these groups provide. MMP-3 and -13 have similar S1′ pockets, which explains why **11c** potently inhibits these enzymes. In contrast, the MMPs possessing either shallow (MMP-1 and -7) or narrow (MMP-9) S1′ pockets[8b] cannot easily accommodate the 4′-bromo-substituted biphenyl ring system, resulting in a loss in binding energy and a decrease in potency.

To identify the best possible candidate for chronic dosing in vivo, we determined the pharmacokinetic parameters in rat for selected compounds from Tables 1 and 2. As summarized in Table 3, it appears that biphenyl derivatives substituted in the 4′-position with nonmetabolizable groups (**11a,c,e,f, j**) provide compounds that achieve high plasma concentrations with long elimination half-lives ($t_{1/2}$ = 34−117 h), compared to **5** ($t_{1/2}$ = 3.35 h), whereas easily metabolized groups (**11g,h**) gave potent inhibitors with very short $t_{1/2}$ (<30 min). Replacement of the methyl group in **11g** with either cyano (**11k**) or nitro (**11m**) increased the $t_{1/2}$ to 12.5 and 19.5 h, respectively, significantly increasing the AUC relative to the unsubstituted analogue, compound **5**.

Since compound **11c** demonstrated the best combination of broad-spectrum inhibition in vitro and pharmacokinetic parameters in vivo, we used the 4′-bromobiphenylsulfonamide portion of **11c** as a template for a second SAR study wherein substitution α to the carboxylic acid moiety was examined (**11n−v**, Table 4). Modeling studies suggested that hydrogen-bonding and aromatic stacking interactions could be formed with amino acid residues at S2 through S4 provided that the inhibitor side chain was of appropriate length. On the basis of this observation, we modified the α-position of **11c** utilizing a variety of amino acids which gave compounds (**11n−v**) that, in general, retained inhibitory activity. Subsequent modeling studies for one of these inhibitors, **11s**, showed that the side chain can reside well into the nonprime region of the catalytic domain, forming hydrogen bonds with the backbone carbonyl of Ala 167 as well as aromatic stacking interactions with
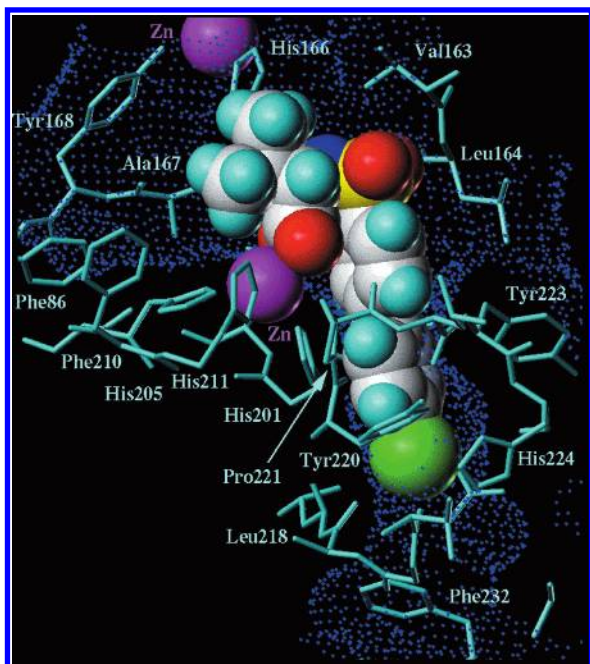
Figure 3. View of a model of **11c** in the active site of MMP-3CD. Amino acid residues that form the binding cleft and the P1′ channel are labeled, and a Connolly surface has been added. Note the relatively spacious, flat P1 site occupied by the isopropyl side chain in contrast to the narrow channel at P1′, into which the 4-bromobiphenyl projects.
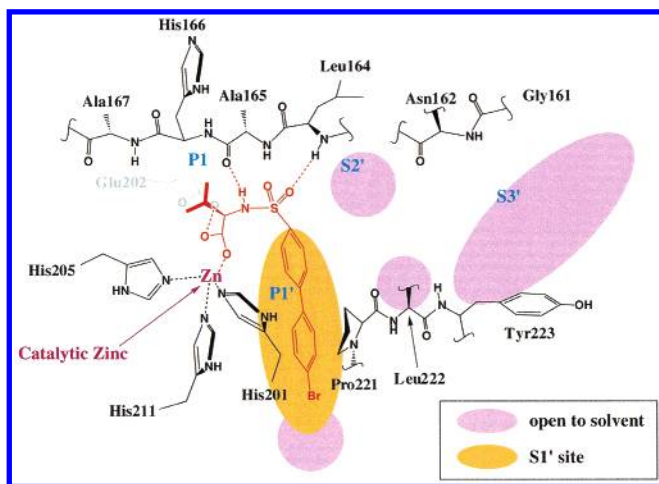

Figure 4. Schematic of the interactions formed between **11c** and MMP-3CD. The S2′ and S3′ sites normally occupied by peptide hydroxamate inhibitors are eschewed in favor of P1′ occupancy by the biphenyl moiety. A tetrahedral ligation geometry of the catalytic zinc is predicted, together with three inhibitor/protein hydrogen bonds.

Tyr 168 (Figure 5). A less lipophilic inhibitor, **11v**, utilized a benzyl sulfone to achieve aromatic stacking with Phe 86. For this compound, a hydrogen bond between one of the sulfone oxygens and the Ala 167 NH significantly contributes to in vitro potency, since the corresponding sulfide **11u**, which lacks this hydrogen bond, is 2−3 times less potent. However, on the basis of the in vitro data presented in Table 4, favorable nonprime interactions are likely to be compromised by increased entropy due to the flexibility of the side chains, since compounds with more rigid, considerably smaller side chains (**11o,p**) are nearly as potent as **11v**.

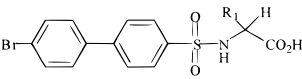Table 5 summarizes the pharmacokinetic parameters for compounds **11n−v**. As shown in Table 5, the

Table 3. Rat Pharmacokinetic Parameters of Substituted Biphenylsulfonamide Derivatives Following a Single 5 mg/kg Oral Cassette Gavage Dose in Rats

compd	C_{max} (μg/mL)	C_{24} (μg/mL)	t_{max} (h)	$t_{1/2}$ (h)	AUC(0−tldc) (μg·h/mL)	AUC(0−∞) (μg·h/mL)
5	5.18	0.039	0.50	3.35	12.1	3.6
11a	18.7	11.3	2.75	45.5	670	1024
11c	42.4	22.7	2	43.6	1401	2822
11e	8.86	4.02	0.50	34.1	170	427
11f	28.5	21.3	1.88	117	1364	4043
11g	3.07	BLQ	0.50	0.403	2.25	2.37
11h	4.26	BLQ	0.50	0.357	2.79	2.98
11j	18.6	11.7	2.25	37.9	685	1112
11k	17.1	5.48	2.67	12.5	289	363
11m	23.4	8.36	0.667	19.5	402	586

differences in lipophilicity attributed to the modification of α-substituents significantly influence the pharmacokinetic activity for compounds **11n−v**. For example, compound **11p** (isobutyl side chain) exhibited good oral absorption in the rat and achieved high plasma concentrations with a long elimination half-live comparable to that of **11c** (Table 3). However, replacement of the isobutyl group with smaller, less lipophilic substituents (methyl in **11o**, hydrogen in **11n**) or with a larger, more lipophilic group (benzyl in **11q**) diminished the C_{max}, $t_{1/2}$, and AUCs relative to **11p**. Incorporation of side chains bearing larger substituents gave compounds (**11r,s,u,v**) that, in general, were poorly absorbed. Of these compounds, only the benzyl sulfide (**11u**) achieved plasma concentrations comparable to those of **11n,o,q**, albeit considerably less than the levels achieved for **11c** or **11p**.

Since the majority of compounds evaluated in these studies were derived from natural (*S*)-amino acids, we synthesized the enantiomer of **11c** and assessed the effects of changing amino acid stereochemistry on biological (Table 6) and pharmacokinetic (Table 7) activity. Enantiomers of analogues with a carboxylate zinc coordinating group (**11c,c′**) were equally effective at inhibiting MMPs. Similarly, a second pair of enantiomers, **11k,k′**, exhibited comparable potency against the majority of the MMPs, although differences were observed for MMP-9 (*R*-isomer is 15-fold more potent than the *S*-isomer). The *S*-stereoisomers achieved higher plasma C_{max} concentrations (Tables 3 and 7, 42.4 μg/mL for **11c** and 17.1 μg/mL for **11k**) compared to the corresponding *R*-enantiomers (25.6 μg/mL for **11c′** vs 12.2 μg/mL for **11k′**) following a single oral dose in rat.

In lieu of crystal structures of **11c** with MMP-3CD, we used crystal structures of analogous MMP-3CD/diphenylpiperidine complexes (ref codes 1ciz and 1caq in the Protein Databank) to rationalize the observed lack of stereoselectivity for inhibitors containing carboxy−zinc binding (Figure 6). As can be seen in Figure 6, the orientation of the sulfonamide moiety is the key interaction allowing these isomers to nearly overlap in the MMP-3CD. The sulfonamide NH in the *S*-isomer hydrogen bonds to the backbone carbonyl of Ala 165. In contrast, the sulfonyl group of the *R*-isomer rotates but maintains its hydrogen bond with Glu 202, which allows the sulfonamide NH to form a water-mediated hydrogen bond to Pro 221 on the opposite side of the binding cleft. This orients the amino acid side chain such that it occupies nearly the same area of space in the P1 site as that of the *S*-isomer, resulting in nearly equipotent isomer pairs.

Table 4. Modification of Substituents Appended to the α-Position of Biphenylsulfonamide Derivatives

compd	R_1	formula[a]	mp (°C)	MMPs IC$_{50}$ (μM)[b]
				1[c]	**2**	**3**[d]	**7**	**9**[c]	**13**
11n	H	$C_{14}H_{12}BrNO_4S$	200−202	50	0.004	0.010	77	6.7	0.026
11o (*S*)	CH$_3$	$C_{14}H_{14}BrNO_4S$	195−196	13	0.012	0.012	11	9.5	0.010
11p (*S*)	CH$_3$CH(CH$_3$)$_2$	$C_{18}H_{20}BrNO_4S$	ND	7.0	0.009	0.007	3.1	4.9	0.005
11q (*S*)	CH$_2$Ph	$C_{21}H_{18}BrNO_4S$	159−161	56	0.019	0.020	100	27	0.021
11r (*S*)	(CH$_2$)$_4$NHCBZ	$C_{26}H_{27}BrN_2O_6S$	151−152	40	0.031	0.028	15	10	0.013
11s (*S*)	(CH$_2$)$_4$NHCO(CH$_2$)$_2$Ph	$C_{27}H_{29}BrN_2O_5S$	198−199	15	0.004	0.010	8.6	4.8	0.004
11t (*S*)	(CH$_2$)$_3$NHCO(CH$_2$)$_2$Ph	$C_{26}H_{27}BrN_2O_5S$	157−159	41	0.008	0.021	6.8	7.7	0.007
11u (*R,S*)	(CH$_2$)$_2$SCH$_2$Ph	$C_{23}H_{22}BrNO_4S_2$	152−154	56	0.007	0.022	36	10	0.036
11v (*R,S*)	(CH$_2$)$_2$SO$_2$CH$_2$Ph	$C_{23}H_{22}BrNO_6S_2$	199−200	27	0.002	0.007	15	2.3	0.012

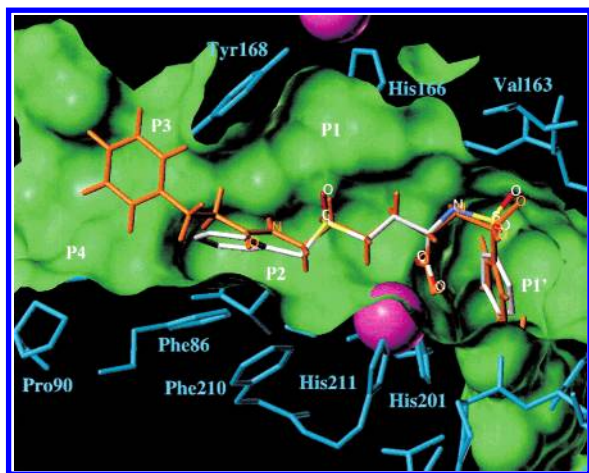[a–d] Refer to footnotes in Table 1. ND denotes not determined.

Figure 5. Predicted binding modes of **11v** (colored by atom type) and **11s** (orange) in MMP-3CD. Each possesses side chains that occupy the P1 through P4 sites of the protein. The terminal phenyl rings of **11s,v** form π−π stacking interactions with Tyr 168 and Phe 86, respectively. Each side chain can form a hydrogen bond to the adjacent protein backbone.

Table 5. Rat Pharmacokinetic Parameters for Analogues of Compound **11c** Following a Single 5 mg/kg Oral Cassette Gavage Dose

compd	C_{max} (μg/mL)	C_{24} (μg/mL)	t_{max} (h)	$t_{1/2}$ (h)	AUC(0−tldc) (μg·h/mL)	AUC(0−∞) (μg·h/mL)
11n	9.96	5.67	8.00	15.6	276	316
11o	17.2	12.9	10.5	25.1	584	818
11p	30.7	12.4	2.33	41.8	578	1211
11q	10.3	6.28	2.67	29.7	310	465
11r	0	−	ND	ND	−	0
11s	0	−	ND	ND	−	0
11u	11.6	1.53	1.33	12.5	119	132
11v	0.451	BLQ	1.67	3.88	2.48	2.73

Having identified a preferred side chain, further work focused on increasing the inhibitory activity for this series utilizing hydroxamic acid as the zinc coordinating moiety (Table 6). In this study, conversion of the carboxylic acid of **11c,k** to the corresponding hydroxamic acids (**16a,b**) unexpectedly decreased in vitro activity in our biological screens. However, evaluation of the hydroxamic acids derived from the corresponding D-amino acids (**16a′,b′**) showed that these compounds potently inhibited all of the MMPs. For the first time in this series, compounds exhibited broad-spectrum inhibitory activity, achieving <200 nM potency vs all of the MMPs in the in vitro screens (Table 6). However,

16a′,b′ had poor systemic availability when dosed orally in vivo (Table 7).

The increased potency observed for *R*- relative to *S*-enantiomers for analogues (Table 6, **16a′,b′**) containing a sulfonamide linker to a hydroxamic acid coordinated to zinc was not well-explained using models based on carboxy-containing inhibitors. Although a crystal structure of **16a′** complexed with MMP-3CD could not be obtained, we were able to cocrystallize the potent *R*-enantiomer from a related diphenyl ether series (**17**, Figure 7) that exhibits a similar in vitro profile (Table 5).[12] From this crystal structure, it can be seen that several hydrogen bonds occur between the protein and inhibitor polar groups, which stabilize the complex formation. The catalytic zinc forms a trigonal bipyramidal coordination with the imidazole nitrogen atoms of three histidines (201, 205, and 211) and two oxygen atoms of the hydroxamic acid. The hydroxamic acid hydroxyl oxygen of **17** is located within hydrogen bond proximity to both carbonyl oxygen atoms of Glu 202 (2.7 and 3.0 Å). One of the sulfonyl oxygen atoms and the NH of the hydroxamic acid of the inhibitor are located within hydrogen-bonding distance to the carbonyl oxygen of Leu 164 (2.8 Å) and the NH of Ala 165 (3.0 Å), respectively. The inhibitor diphenyl ether comfortably occupies approximately two-thirds of the deep S1′ hydrophobic channel.

Surprisingly, the MMP-3CD/compound **17** complex (Figure 7) contained a second bound inhibitor molecule together with a third Zn^{2+} ion (Zn3). This zinc forms a trigonal bipyramidal complex with two hydroxamic acid oxygen atoms of **17**, His 224 Nδ, Nε of His 96 from a symmetry-related protein molecule, and an oxygen atom of a water molecule that is positioned between Zn3 and Glu 137 from the symmetry-related molecule. Although the majority of atoms from this second inhibitor molecule are exposed to the surface, its distal phenyl ring partially occupies the 'exit' of the S1′ channel, as if plugging it. Binding of this second inhibitor molecule is considered to be an artifact of crystal packing and is unlikely to occur in solution.

A comparison of the binding mode for the hydroxamic acid **17** (crystal structure) and the carboxylic acid **11c** (overlayed via modeling) with MMP-3 is shown in Figure 8. Consistent with both structures, secondary interactions with the enzyme are highly dependent on the compound's ability to ligate the active-site zinc. For

Table 6. Effects of Stereochemistry on the In Vitro Activity for Carboxylic Acid and Hydroxamic Acid Biphenylsulfonamides

						MMPs IC$_{50}$ (μM)[b]					
compd	R	R$_2$	formula[a]	mp (°C)	1[c]	2	3[d]	7	9[c]	13
11c (*S*)	Br	OH	C$_{17}$H$_{18}$BrNO$_4$S	192–193	6.0	0.004	0.007	7.2	7.9	0.008
11c′ (*R*)	Br	OH	C$_{17}$H$_{18}$BrNO$_4$S	192–193	6.2	0.005	0.008	11	1.5	0.016
11k (*S*)	CN	OH	C$_{17}$H$_{18}$N$_2$O$_4$S	182–183	18	0.033	0.006	7.0	59	0.037
11k′ (*R*)	CN	OH	C$_{17}$H$_{18}$N$_2$O$_4$S	181–182	14	0.007	0.005	19	3.8	0.053
16a (*S*)	Br	NHOH	C$_{17}$H$_{19}$BrN$_2$O$_4$S[e]	169–170	24	0.45	0.81	78	84	0.65
16a′ (*R*)	Br	NHOH	C$_{17}$H$_{19}$BrN$_2$O$_4$S	167–168	0.11	0.001	0.005	0.14	0.018	0.002
16b (*S*)	CN	NHOH	C$_{18}$H$_{19}$N$_3$O$_4$S[f]	156–157	29	0.53	0.135	16	100	0.58
16b′ (*R*)	CN	NHOH	C$_{18}$H$_{19}$N$_3$O$_4$S	154–156	0.17	0.001	0.005	0.24	0.027	0.001
17 (*R*)				150	0.05	0.001	0.004	0.18	0.003	0.002

[a–d] Refer to footnotes in Table 1. [e] Anal. C: calcd 47.78, found 48.21; H: calcd 4.48, found 4.58; N: calcd 6.56, found 6.33. [f] Contains 0.32H$_2$O (98.5% parent).
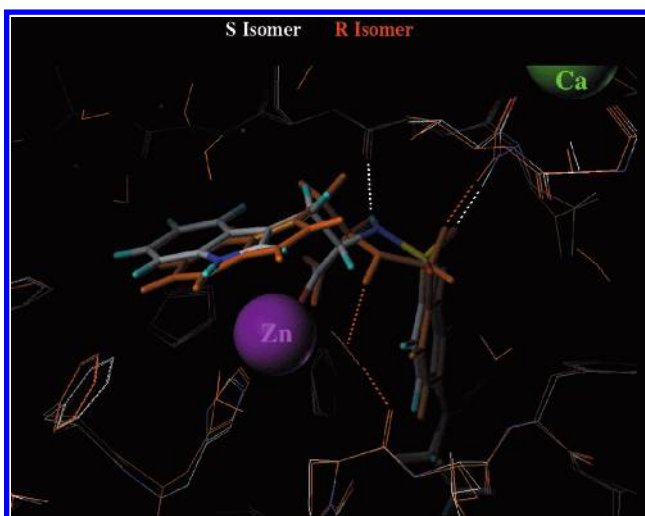

Figure 6. Recently reported[13] crystal structures of the *R*- and *S*-stereoisomers of related diphenylpiperidine MMP inhibitors containing a Trp side chain at P1. The inhibitor sulfonamide NH in the *R*-isomer (orange) eschews a hydrogen bond to Ala 165 in favor of a water-bridged hydrogen bond to the backbone carbonyl of Pro 221. This allows the Trp to occupy the P1 site in each case. The isomers are equipotent against MMP-3CD.

Table 7. Pharmacokinetic Parameters of Carboxylic Acid and Hydroxamic Acid Derivatives Following a Single 5 mg/kg Oral Cassette Gavage Dose

compd	C_{max} (μg/mL)	C_{24} (μg/mL)	t_{max} (h)	$t_{1/2}$ (h)	AUC(0–tldc) (μg·h/mL)	AUC(0–∞) (μg·h/mL)
11c′	25.6	16.3	4.5	41.7	924	1385
11k′	12.2	4.49	1.33	12.8	256	277
16a′	5.93	0.01	0.33	6.78	5.73	5.86
16b′	0.18	0	1	0.79	0.23	0.33
17	0.31	0	0.33	7.78	2.17	3.17

compound **17**, the hydroxamic acid interacts strongly and specifically in the active site, forming four strong electrostatic interactions. As a result, the bond vector between it and the α-carbon position has little opportunity for conformational flexibility to accommodate alternate linkers and/or hydrophobic groups at S1′. This fact, coupled with the size of the hydroxamic acid group (four heavy atoms), forces an alternate pucker in the sulfonamide linker, resulting in a shift of the sulfonyl group, such that the oxygen is now equidistant from the

backbone NH of Leu 164 and Ala 165. The resulting bond vector in **17** allows the α-isopropyl group to be projected toward the S1 site. However, under these steric constraints the isopropyl group in the *S*-isomer is predicted to be oriented back toward, and in steric contact with, the β-sheet that forms the upper rear of the binding cleft, which would result in a significant loss in potency. In contrast, the carboxylic acid group (three heavy atoms) of **11c** interacts less strongly, forming only two strong electrostatic interactions with the protein, and therefore allows some latitude in the position of bond vector to the isopropyl group. The smaller carboxyl group allows a reorientation of the side chain such that both enantiomers (*R*-isomer) can occupy nearly the same area of space in the P1 site.

On the basis of its potent inhibitory activity in vitro, pharmacokinetics in vivo, and physicochemical properties, we selected compound **11c** for further testing. Specificity testing demonstrated that **11c** was selective for MMPs, since it was shown to be inactive, at 100 μM, against a total of 25 enzymes and receptors including ACE, ECE, IL-1, and TACE. Furthermore, subsequent pharmacokinetic studies showed that compound **11c** exhibited good oral pharmacokinetic profile in three species, achieving plasma C_{max} concentrations in the rat, dog, and monkey (62, 73, and 7 μM, respectively) following chronic oral dosing (3 mg/kg/day for 2 weeks).

Conclusions

In summary, we have examined the SAR for a series of biphenylsulfonamide derivatives from which **11c** was identified as a selective inhibitor of MMPs, exhibiting nanomolar potency against MMP-2, -3, and -13 and micromolar potency vs MMP-1, -7, and -9. For this series of compounds, we showed that replacement of the carboxylic acid of **11c** with a hydroxamic acid functionality (**16a**) surprisingly decreased in vitro activity compared to **11c**. In contrast, the enantiomer of **16a** (**16a′**) gave the best in vitro profile of compounds evaluated in this series, achieving broad-spectrum inhibitory activity (nanomolar potency) against each of the MMPs in our biological screens. Subsequent structural analysis utilizing X-ray crystallography, complemented by computer modeling, identified key enzyme/
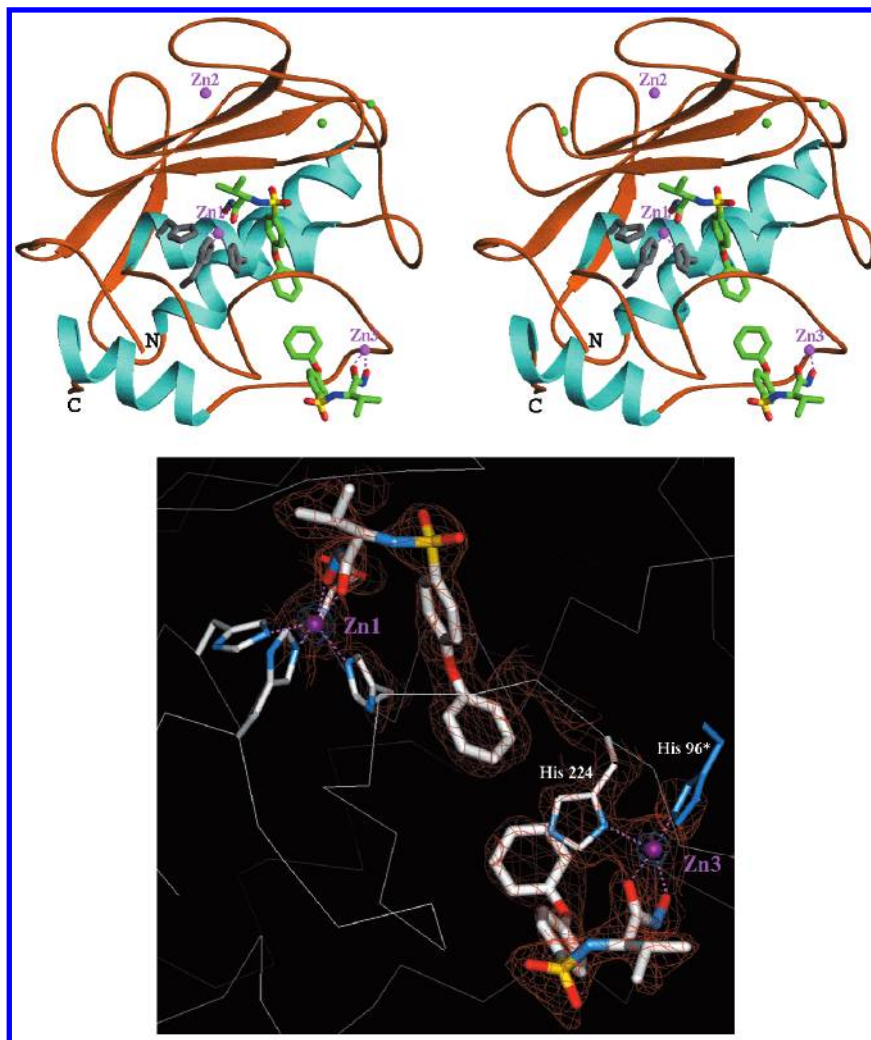
Figure 7. Crystal structure of **17** in MMP-3CD. Similar to the *R*-isomer of the diphenylpiperidine in Figure 6, a direct inhibitor sulfonamide NH to protein hydrogen bond is not formed.

inhibitor interactions that are predicted to contribute to this stereoselectivity. Unfortunately, **16a′** exhibited poor oral pharmacokinetics. Compound **11c,** however, displayed the best pharmacokinetics of compounds evaluated in this series, achieving plasma concentrations in rat, dog, and monkey, exceeding its IC$_{50}$ values against most of the MMPs in the in vitro screens (Table 1). On the basis of its biological and pharmacokinetic activity, compound **11c** (PD 166793) was used as a tool to investigate the role of MMPs in various diseases. Subsequent pharmacological studies will be the subject of future reports from these laboratories.

Experimental Section

General Methods. All commercially available starting materials and solvents were reagent grade. Solutions containing products were dried over anhydrous magnesium sulfate (MgSO$_4$). Melting points were determined on a Thomas-Hoover melting point apparatus and are uncorrected. Analytical thin-layer chromatography (TLC) was carried out using Merck DC-F$_{254}$ precoated silica gel plates. Flash chromatography was performed using kieselgel 60 (230−400 mesh) silica gel. ^{1}H NMR spectra were recorded on a Varian Gemini 300-MHz instrument using CDCl$_3$ or DMSO-d_6 as the solvent, reporting the chemical shifts in parts per million (ppm). Mass spectra was determined on a Finnigan TSQ-70 mass spectrometer (CI mode). Elemental analysis were determined by Robertson-Microlit Laboratories Inc., NJ, and are within ±0.4% of the calculated values unless otherwise noted.

General Procedure for Preparing Substituted Biphenylsulfonamide Derivatives (Method A). Synthesis of (*S*)-3-Methyl-2-(4′-methylbiphenyl-4-sulfonylamino)butyric Acid (11g). (*S*)-2-(4-Bromobenzenesulfonylamino)-3-methylbutyric Acid, *tert*-Butyl Ester (8). To a suspension of 4-bromobenzenesulfonyl chloride **(6)** (20 g, 0.078 mol) and L-valine, *tert*-butyl ester hydrochloride **(7)** (16.4 g, 0.078 mol) in aqueous tetrahydrofuran (1:1, 400 mL) was added dropwise triethylamine (15.7 g, 0.156 mol). The reaction mixture was stirred at room temperature for 16 h, followed by the addition of ethyl acetate (300 mL) and aqueous HCl (1 M, 300 mL). The organic phase was separated, dried, and concentrated in vacuo leaving a white solid. Recrystallization of the crude product from hexane/ethyl acetate provided compound **8** (19.7 g, 67%) as a white crystalline solid: mp 108−110 °C; ^{1}H NMR (CDCl$_3$) δ 7.7 (d, 2H), 7.6 (d, 2H), 5.1 (d, 1H), 3.6 (m, 1H), 2.0 (m, 1H), 1.2 (s, 9H), 0.9 (d, 3H), 0.8 (d, 3H) ppm; CI-MS *m*/*e* 391. Anal. (C$_{15}$H$_{22}$BrNO$_4$S) C, H, N.

(*S*)-3-Methyl-2-(4′-methylbiphenyl-4-sulfonylamino)-butyric Acid, *tert*-Butyl Ester (10g). A solution of compound **8** (15 g, 0.039 mol) and 4-methylbenzeneboronic acid (6.4 g, 0.048 mol) in toluene (150 mL) was treated with tetrakis-(triphenylphosphine)palladium(0) (0.75 g) and aqueous sodium carbonate (7.5 g, 75 mL H$_2$O), respectively. The reaction mixture was refluxed for 72 h, cooled, and diluted with ethyl acetate (250 mL) and aqueous HCl (1 M, 250 mL). The mixture was filtered through a pad of Celite, followed by separation of the organic phase from the aqueous layer. The organic solution was washed with brine, dried, and concentrated in vacuo to give a yellow-brown solid. The crude product was triturated with hexane/ethyl acetate (4:1) to give compound **10g** (11.5 g,
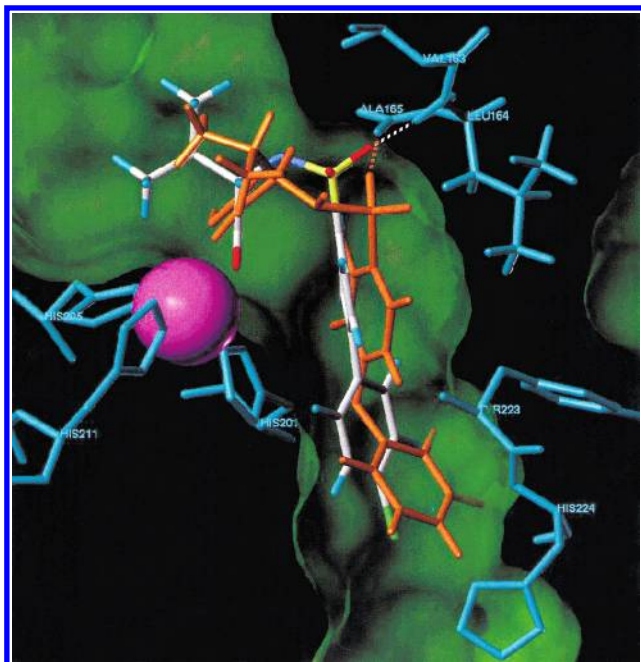
Figure 8. Overlay of the MMP-3CD/**17** crystal structure (orange) and the model of **11c**. The *S*-isomer of **17** would be expected to project the isopropyl group back into the protein, clashing sterically. The marked reduction in potency of the *S*-isomers of the present biphenyl series is consistent with this binding mode. Hydrogens have been added to Leu 164 and Ala 165 to illustrate inhibitor to protein hydrogen bonds that are formed.

72%) as a white solid: mp 168−169 °C; ^{1}H NMR (CDCl$_3$) δ 7.8 (d, 2H), 7.6 (d, 2H), 7.4 (d, 2H), 7.2 (d, 2H), 5.1 (d, 1H), 3.6 (dd, 1H), 2.4 (s, 3H), 2.0 (m, 1H), 1.1 (s, 9H), 1.0 (d, 3H), 0.8 (d, 3H) ppm; CI-MS *m*/*e* 402. Anal. (C$_{22}$H$_{29}$NO$_4$S) C, H, N.

(*S*)-3-Methyl-2-(4′-methylbiphenyl-4-sulfonylamino)-butyric Acid (11g). To a solution of anisole (2.6 g, 0.024 mol) in trifluoroacetic acid (100 mL) was added compound **10g** (11 g, 0.027 mol) in portions over a period of 10 min. The solution was stirred at room temperature for 14 h, then poured over ice. The resulting white precipitate was collected by filtration and recrystallized from hexane/ethyl acetate to give **11g** (6.3 g, 67%) as a crystalline white solid: mp 191−193 °C; ^{1}H NMR (DMSO-*d*$_6$) δ 8.0 (d, 1H), 7.8 (s, 3H), 7.6 (d, 2H), 7.3 (d, 2H), 3.5 (m, 1H), 2.4 (s, 3H), 1.9 (m, 1H), 0.8 (dd, 6H) ppm; CI-MS *m*/*e* 347. Anal. (C$_{18}$H$_{21}$NO$_4$S) C, H, N.

Compounds **11a,b**,**h**,**j**−**l** were also synthesized from **6** utilizing similar reaction conditions.

Alternative Procedure for Preparing Substituted Biphenylsulfonamide Derivatives (Method B). Synthesis of (*S*)-2-(4′-Bromobiphenyl-4-sulfonylamino)-3-methylbutyric Acid (11c). 4′-Biphenyl-4-sulfonic Acid (13c). To a stirred solution of 4-bromobiphenyl **(12c)** (140 g, 0.60 mol) in chloroform (1.4 L) was added dropwise at room temperature chlorosulfonic acid (84 g, 0.72 mol). During the addition of chlorosulfonic acid, a white solid precipitated. The reaction mixture was stirred at room temperature for 4 h, at which time the precipitate was collected by filtration and washed with cold chloroform. The product was oven-dried at 40 °C to a constant weight to give **13c** (142 g, 75%) as a white solid. The crude product was used in the next step without further characterization.

4′-Bromobiphenyl-4-sulfonyl Chloride (14c). The crude sulfonic acid derivative **13c** (142 g, 0.60 mol) was diluted with thionyl chloride (600 mL) and treated with a catalytic amount of *N*,*N*-dimethylformamide (0.5 mL). The reaction mixture was refluxed for 4 h, cooled to room temperature, and concentrated in vacuo. To remove residual thionyl chloride, toluene was added and was concentrated in vacuo. The resulting yellow residue was recrystallized from hexane/ethyl acetate to yield

the sulfonyl chloride **14c** (106 g, 71%) as a crystalline white solid: mp 122−124 °C; ^{1}H NMR (CDCl$_3$) δ 8.1 (d, 2H), 7.7 (d, 2H), 7.6 (d, 2H), 7.5 (d, 2H) ppm. Anal. (C$_{12}$H$_8$BrClO$_2$S) C, H.

(*S*)-2-(4′-Bromobiphenyl-4-sulfonylamino)-3-methylbutyric Acid, *tert*-Butyl Ester (10c). A mixture of L-valine, *tert*-butyl ester hydrochloride (63.2 g, 0.30 mol) and the sulfonyl chloride derivative **14c** (100 g, 0.30 mol) in aqueous tetrahydrofuran (1:1, 1 L) was treated dropwise with 2 equiv of triethylamine (61 g, 0.60 mol). The reaction mixture was stirred at room temperature for 45 min, followed by the addition of ethyl acetate (500 mL) and aqueous HCl (1 M, 500 mL), respectively. The organic phase was separated, dried, and concentrated in vacuo. The residue was triturated with hexane and collected by filtration to give **10c** (134 g, 95%) as a white solid: mp 131−133 °C; ^{1}H NMR (CDCl$_3$) δ 7.9 (d, 2H), 7.6 (dd, 4H), 7.4 (d, 2H), 5.1 (d, 1H), 3.6 (dd, 1H), 2.0 (m, 1H), 1.1 (s, 9H), 1.0 (d, 3H), 0.8 (d, 3H) ppm. Anal. (C$_{21}$H$_{26}$BrNO$_4$S) C, H, N.

(*S*)-2-(4′-Bromobiphenyl-4-sulfonylamino)-3-methylbutyric Acid (11c). To a stirred solution of anisole (30 g, 0.28 mol) in trifluoroacetic acid (560 mL) was added compound **10c** (130 g, 0.28 mol). The reaction mixture was stirred at room temperature for 4 h and poured over ice (1 L), and the resulting precipitate was collected by filtration. The crude product was washed with ice-cold water and oven-dried to a constant weight. The powder was recrystallized from hexane/ethyl acetate to yield **11c** (76 g, 67%) as a crystalline white solid: mp 191−193 °C; ^{1}H NMR (CDCl$_3$) δ 7.7 (d, 2H), 7.5 (d, 2H), 7.4 (d, 2H), 7.3 (d, 2H), 5.9 (d, 1H), 3.5 (dd, 1H), 1.9 (m,1H), 0.8 (d, 3H), 0.7 (d, 3H) ppm; CI-MS *m*/*e* 412. Anal. (C$_{17}$H$_{18}$BrNO$_4$S) C, H, N.

Compounds **5** and **11c′−f,i,m,p,q** were synthesized utilizing similar reaction conditions. Esters **10n,o,r−v** required the following base hydrolysis conditions to obtain the corresponding acids **11n,o,r−v**.

Synthesis of (±)-4-Benzylsulfanyl-2-(4′-bromobiphenyl-4-sulfonylamino)butyric Acid (11u). The methyl ester **10u** (2 g, 3.7 mmol) was suspended in *p*-dioxane/water (1:1, 70 mL) followed by the addition of lithium hydroxide monohydrate (0.47 g, 11.2 mmol) in one portion. The reaction mixture was stirred at room temperature for 16 h, then diluted with water (100 mL). The suspension was acidified with concd HCl (pH = 1) and the product was extracted with ethyl acetate (100 mL). The organic extract was dried and concentrated in vacuo leaving a white solid. The crude product was triturated with hexane/ethyl acetate (9:1) and collected by filtration to give the carboxylic acid **11u** (1.4 g, 72%): mp 152−154 °C; ^{1}H NMR (CDCl$_3$) δ 7.8 (d, 2H), 7.5 (d, 2H), 7.4 (d, 2H), 7.3 (d, 2H), 7.2−7.0 (m, 5H), 6.1 (d, 1H), 3.8 (m, 1H), 3.5 (s, 2H), 2.3 (t, 2H), 1.9 (m, 1H), 1.8 (m,1H) ppm; CI-MS *m*/*e* 537. Anal. (C$_{23}$H$_{22}$BrNO$_4$S$_2$) C, H, N.

General Procedure for Preparing Hydroxamic Acid Derivatives (Method C). Synthesis of (*R*)-2-(4′-Bromobiphenyl-4-sulfonylamino)-*N*-hydroxy-3-methylbutyramide (16a′). To a solution of **11c′** (0.35 g, 0.85 mmol) in dichloromethane (5 mL) was added in one portion oxalyl chloride (0.43 g, 3.4 mmol). *N*,*N*-Dimethylformamide was added as a catalyst. The solution was stirred at room temperature for 2 h, at which time the solvent was concentrated in vacuo. The resulting solid was suspended in hexane and collected by filtration. The crude sulfonyl chloride (0.36 g, 0.85 mmol) was diluted with tetrahydrofuran (5 mL) followed by the dropwise addition of a solution of *O*-2-tetrahydro-2*H*-pyranhydroxylamine (0.2 g, 1.7 mmol) in tetrahydrofuran (5 mL). The reaction mixture was stirred at room temperature for 1 h, followed by the addition of ethyl acetate (10 mL) and aqueous HCl (1 M, 5 mL). After stirring the mixture for 14 h, the layers were separated and the organic phase washed with brine, dried, and concentrated in vacuo. The resulting solid was suspended in hexane/ethyl acetate and collected by filtration to give **16a′** (0.12 g, 33%) as a white solid: mp 167−168 °C dec; ^{1}H NMR (DMSO-*d*$_6$) δ 10.5 (s,1H), 8.8 (bs, 1H),

8.0 (d, 1H), 7.8 (s, 4H), 7.7 (s, 4H), 3.3 (m, 1H), 1.8 (m, 1H), 0.7 (m, 6H) ppm; CI-MS m/e 428. Anal. ($C_{17}H_{19}BrN_2O_4S$) C, H, N.

Compounds **16a**,**b**,**b′** in Table **5** were synthesized in a similar manner.

Metalloproteinase Inhibition Assays. Assays used human MMPs expressed either as catalytic domains (CDs) or as full-length (FL) forms. The CDs of gelatinase A (MMP-2), stromelysin (MMP-3), matrilysin (MMP-7), and collagenase-3 (MMP-13) were expressed in bacteria and purified chromatographically. FL collagenase (MMP-1) and gelatinase B (MMP-9) were purified from human cell-conditioned media and activated by respective exposure to trypsin or MMP-3CD before diluting to assay concentrations. Typical assays were buffered to pH 7.0, with the exception of MMP-3CD (pH 6.0), with 50 mM HEPES (exception: MMP-2CD used MOPS) and contained 10 mM $CaCl_2$, 1 mM 5,5′-dithiobis(2-nitrobenzoic acid) (DTNB), 100 μM Ac-Pro-Leu-Gly-thioester-Leu-Leu-Gly-Oet substrate (MMP-9 used 50 μM), 0.1% Brij 35 detergent, 2% DMSO vehicle, various concentrations of test compound, and adequate enzyme (2.5−50 nM) to provide measurable activity in a 10-min reaction. The MMP-2CD assay also contained 10 μM $ZnCl_2$. Enzyme-catalyzed reactions (100 μL total volume) were monitored spectrophotometrically for 10 min using a 96-well microplate reader by following a change in absorbance at 405 nm that occurs upon reaction of liberated thiol with DTNB following substrate hydrolysis. The rates of changes at A_{405} were recorded as measures of the reaction velocities. Blank reaction rates (without enzyme) are negligible under these conditions. The percent of uninhibited control activity was calculated for each reaction using the equation: % control activity = (inhibited rate/control rate) × 100. IC_{50} values were calculated by least-squares regression analysis fitting the percent of control activity vs inhibitor concentration data to the sigmoid inhibition equation: % control activity = $100/[1 + ([I]/IC_{50})^{slope}]$, where [I] is the inhibitor concentration, IC_{50} is the concentration of inhibitor where the reaction rate is 50% inhibited relative to the control reaction rate, and slope is the value of the slope of the curve at its inflection point. Replicate IC_{50} values were averaged to obtain the tabulated values.

Human MMP-3 is unique in that it displays a sharp pH optimum between 5.5 and 6.5, with the catalytic activity at pH 7 less than one-third that observed at pH 6.0.[18] The distinct pH profile appears to be an intrinsic characteristic of the human enzyme since it has been reported for the full length and catalytic domain and has been demonstrated for both peptidic and macromolecular substrates.[15,16,23,24] This may represent an important method of posttranslational regulation for the human enzyme since MMP-3 activates more readily and binds TIMP less tightly at acidic pH.[25] As a result of this acidic dependence of activity, the assay employing human MMP-3 was run at pH 6.0.

Molecular Modeling. Models of MMP-3 CD complexed with biphenyl inhibitors containing carboxylic acid zinc chelating groups were constructed based on the crystal structure of a related MMP-3/diphenylpiperidine complex (1caq in the Protein Databank).[13] The diphenylpiperidine portion of the inhibitor from this complex was replaced by the biphenyl moiety of the present inhibitors, keeping the acyclic zinc binding side chain containing the sulfonamide group in its crystallographically observed conformation. Modeling was carried out using SYBYL.[26] Hydrogens were added to the complex, and STO-3G charges were calculated for all inhibitors using Spartan.[27] An 8 Å subst_sphere was defined around the inhibitor, and residues outside this region were aggregated. In addition, the catalytic zinc and its ligating atoms (imidazole nitrogens from His 201, 205, and 211 plus one carboxyl oxygen of the inhibitor) were separately aggregated to preserve the local coordination geometry. Minimization was run via MAXI-MIN using the Tripos force field, all atoms included, Kollman all-atom charges on the protein, and a convergence criteria of 0.01 kcal/mol change in energy gradient. Models of MMP-3CD containing biphenyl inhibitors with hydroxamic acid zinc chelating groups were constructed using a similar protocol, except the acyclic zinc binding side chain conformation from the MMP-3/U24522 crystal structure was used as a starting point.[20]

X-ray Crystallography. Prior to crystallization, a solution containing 0.7 mg/mL MMP-3CD, 5 mM $ZnCl_2$, 5 mM $CaCl_2$, and 20 mM Tris HCl buffer (pH 7.0) was mixed with a solution of 0.8 mg of inhibitor in 30 μL of DMSO. The resulting solution was concentrated 20 times. Equal volumes of complex and resevoir solution containing 1.4 M sodium acetate and 100 mM sodium cacodilate (pH 6.5) buffer were mixed and equilibrated in the hanging drop against a reservoir solution. The crystals grew in space group $P6_522$, $a = b = 74.6$ Å, $c = 139.9$ Å, and one molecule per asymmetric unit. The space group was subsequently confirmed when a correct translation function solution was found. Diffraction data up to 2.1 Å resolution were collected on the 17ID IMCA station at the Advanced Photon Source (APS)[28] using MAR160 CCD. Data were processed and scaled with HKL2000 package.[29]

The structure was solved by molecular replacement using AmoRe.[30] The MMP-3CD protein from a previously published crystal complex (PDB code 1B8Y) was used as a probe. The final model of the complex, obtained after several cycles of refinement by XPLOR,[31] comprised residues 83−250, three Zn^{2+} ions, three Ca^{2+} ions, an inhibitor molecule bound in the active site, a second inhibitor molecule located on the interface between two symmetry-related neighboring protein molecules, and 89 water molecules.

Pharmacokinetic Method. The pharmacokinetic profile was characterized following oral administration in rats. To improve the efficiency of pharmacokinetic screening, a cassette dosing format was used for these studies in which a cocktail of 5−7 compounds were administered together. Compounds were selected for cassette dosing in rat based on their in vitro MMP inhibition profile and structural diversity. The MS/MS fragmentation profile was characterized on a Micromass Quattro II triple quadrupole mass spectrometer. Compounds were grouped for co-administration based on the uniqueness of their MS/MS profiles.

The data reported was collected over a period of months from different cassette dosing experiments. In each study a single 5 mg/kg/compound cocktail was administered to 3 fasted MaleWistar rats (80−90 days old) by oral gavage. The dose suspension was prepared in methyl cellulose. Heparanized plasma samples were collected from a jugular vein cannula at predose, 0.25, 0.5, 1, 2, 3, 4, 6, 8, 12, 24 and 48 h postdose. Plasma was stored frozen at −20 °C until analyzed by LC−MS/MS.

The standards prepared were also a cocktail of the same compounds administered to the rat in the cassette dose. Each compound (5 mg/kg) was dissolved in 10 mL of methanol to prepare separate 500 μg/mL solutions. Appropriate amounts of each stock solution were then added together and diluted volumetrically in methanol to obtain the standard curve. These solutions were later diluted in plasma during the extraction procedure to prepare working standards. The lower limit of quantitation for the assays was 10 ng/mL. All internal standard solutions had a concentration of 5 μg/mL of methanol. The choice of an internal standard was dependent upon optimized chromatographic and/or mass spectrographic conditions.

The pharmacokinetic parameter values were estimated by noncompartmental analysis of individual rat plasma concentration−time data. Maximum plasma concentrations (C_{max}) and times for those to occur (t_{max}) were recorded as observed. Terminal elimination-rate constants (λz) were estimated as the absolute value of the slope of the least-squares linear regression of plasma concentration versus time profiles during the apparent terminal phase. Apparent terminal elimination-half-life values ($t_{1/2}$) were calculated as $0.693/\lambda z$. The area under the plasma concentration−time curve [AUC(0−tldc) and AUC-(0−∞)] values were calculated from time zero to the time of the last detectable concentration (tldc) by using the trapezoidal rule and were extrapolated to infinity (WinNonlin, Version 1.5).

References

(1) Matrisian, L. M. The Matrix Degrading Proteinases. *Bioessays* **1992**, *14*, 455−463.

(2) Denhardt, D. T.; Feng, B.; Edwards, D. R.; Cocuzzi, E. T.; Malyankar, U. M. Tissue Inhibitor of Metalloproteinases (TIMP, aka EPA): Structure, Control of Expression and Biological Function. *Pharmacol. Ther.* **1993**, *59*, 329−341.

(3) Firestein, G. S.; Paine, M. M.; Littman, B. H. Gene Expression (Collagenase, Tissue Inhibitors of Metalloproteinase, Complement and HLA-DR) in Rheumatoid and Osteoarthritic Synovium. *Arthritis Rheum.* **1991**, *34*, 1094−1105.

(4) Pyke, C.; Ralfkiaer, E.; Huhtala, P.; Hurskainen, T.; Danoe, K.; Tryggvason, K. Localization of Messenger RNA for Mr 72,000 and 92,000 Type IV Collagenases in Human Skin Cancers by in situ Hybridization. *Cancer Res.* **1992**, *52*, 1336−1341.

(5) Thompson, R.; Parks, W. Role of Matrix Metalloproteinases in Abdominal Aortic Aneurysms. *Ann. NY Acad. Sci.* **1996**, *800*, 157−174.

(6) Thomas, C. V.; Coker, M. L.; Zellner, J. L.; Handy, J. R.; Crumbly, A. J.; Spinale, F. G. Increased Matrix Metalloproteinase Activity and Selective Upregulation in LV Myocardium from Patients with End-Stage Dilated Cardiomyopathy. *Circulation* **1998**, *97*, 1708−1715.

(7) Nagase, H. Matrix Metalloproteinases. In *Zinc Metalloproteinases in Health and Disease*; Hooper, N. M., Eds.; Taylor and Francis: London, 1996; pp 153−204.

(8) (a) Nagase, H. Activation Mechanisms of Matrix Metalloproteinases. *Biol. Chem.* **1997**, *378*, 151−160. (b) Massova, I.; Kotra, L. P.; Fridman, R.; Mobashery, S. Matrix Metalloproteinases: Structures, Evolution, and Diversification. *FASEB* **1998**, *12*, 1075−1095.

(9) (a) Babine, E. R.; Bender, S. L. Molecular Recognition of Protein−Ligand Complexes: Application to Drug Design. *Chem. Rev.* **1997**, *97*, 1359−1472. (b) Shuker, S.; Hajduk, P.; Meadows, R.; Fesik, S. Discovering High Affinity Ligands for Proteins: SAR by NMR. *Science* **1996**, *274*, 1531−1534.

(10) Beckett, R. P.; Whittaker, M. Matrix Metalloproteinase Inhibitors 1998. *Exp. Opin. Ther. Patents* **1998**, *8*, 259−282.

(11) Whittaker, M.; Brown, P. Recent Advances in Matrix Metalloproteinase Inhibitor Research and Development. *Curr. Opin. Drug Discuss.* **1998**, *1*, 157−164.

(12) Tamura, Y.; Watanabe, F.; Nakatani, T.; Yasui, K.; Fuji, M.; Komurasaki, T.; Tsuzuki, H.; Maekawa, R.; Yoshioka, T.; Kawada, K.; Sugita, K.; Ohtani, M. Highly Selective and Orally Active Inhibitors of Type IV Collagenase (MMP-9 and MMP-2): *N*-Sulfonylamino Acid Derivatives. *J. Med. Chem.* **1998**, *41*, 640−649.

(13) Pavlovsky, A.; Ye, Q. Z.; Ortwine, D.; Humblet, C.; Purchase, C.; White, A.; Roth, B.; Johnson, L.; Hupe, D.; Williams, M.; Dhanaraj, V.; Blundell, T. X-ray Structure of Human Stromelysin Catalytic Domain Complexed with Non-Peptide Inhibitors: Implications for Inhibitor Selectivity. *Protein Sci.* **1999**, *8*, 1455−1462. Entry 1caq in the Protein Databank.

(14) Miyaura, N.; Yanagi, T.; Suzuki, A. The Palladium-Catalyzed Cross-Coupling Reaction of Phenylboronic Acid with Haloarenes in the Presence of Bases. *Synth. Commun.* **1981**, *11*, 513−519.

(15) Wilhelm, S. M.; Shao, Z. H.; Housely, T. J.; Seperack, P. K.; Baumann, A. P.; Gunja-Smith, Z.; Woessner, J. F. Matrix Metalloproteinase-3 (Stromelysin-1). Identification as the Cartilage Acid Metalloprotease and Effect of pH on Catalytic Properties and Calcium Affinity. *J. Biol. Chem.* **1993**, *268*, 21906−21913.

(16) Holman, C.; Kan, C. C.; Gehring, M.; Van Wart, H. Role of His-224 in the Anomolous pH Dependence of Human Stromelysin-1. *Biochemistry* **1999**, *38*, 677−681.

(17) Johnson, L. L.; Pavlovsky, A. G.; Johnson, A. R.; Hupe, D. J.; Janowicz, J. A.; Man, C.-F.; Ortwine, D. F.; Purchase, C. F., III; White, A. D. A Rationalization of the Acidic pH Dependence for Stromelysin-1 (MMP-3) Catalysis and Inhibition. *J. Biol. Chem.*, submitted.

(18) Johnson, L.; Bornemeier, D.; Janowicz, J.; Chen, J.; Pavlovsky, A.; Ortwine, D. Effect of Species Differences on Stromelysin-1 (MMP-3) Inhibitor Potency: An Explanation of Inhibitor Selectivity Using Homology Modeling and Chimeric Proteins. *J. Biol. Chem.* **1999**, *274*, 24881−24887.

(19) Parker, M. H.; Lunney, E. A.; Ortwine, D. F.; Pavlovsky, A. G.; Humblet, C.; Brouillette, C. G. Analysis of the Binding of Hydroxamic Acid and Carboxylic Acid Inhibitors to the Stromelysin-1 (Matrix Metalloproteinase-3) Catalytic Domain by Isothermal Titration Calorimetry. *Biochemistry* **1999**, *38*, 13592−13601.

(20) Dhanaraj, V.; Ye, Qui-Zhuang; Johnson, L. L.; Hupe, D. J.; Ortwine, D. F.; Dunbar, J. B., Jr; Rubin, J. R.; Pavlovsky, A.; Humblet, C.; Blundell, T. L. X-ray Structure of a Hydroxamate Inhibitor Complex of Stromelysin Catalytic Domain and its Comparison with Members of the Zinc Metalloproteinase Superfamily. *Structure* **1996**, *4*, 375−386.

(21) Massova, I.; Fridman, R.; Mobashery, S. Structural Insights into the Catalytic Domains of Human Matrix Metalloprotease-2 and Human Matrix Metalloprotease-9: Implications for Substrate Specificities. *J. Mol. Model.* [*Electronic Publication*] **1997**, *3*, 17−30.

(22) Lovejoy, B.; Welch, A. R.; Carr, S.; Luong, C.; Broka, C.; Hendricks, R. T.; Campbell, J. A.; Walker, K.; Martin, R.; Van Wart, H.; Browner, M. Crystal Structures of MMP-1 and MMP-13 Reveal the Structural Basis for Selectivity of Collagenase Inhibitors. *Struct. Biol.* **1999**, *6*, 217−221.

(23) Ye, Q. Z.; Johnson, L.; Hupe, D. J.; Baragi, V. Purification and Characterization of the Human Sromelysin Catalytic Domain Expressed in *Escherichia coli. Biochemistry* **1992**, *31*, 11231−11235.

(24) Harrison, R. K.; Chang, B.; Niedzwiecki, L.; Stein, R. L. Mechanistic Studies on the Human Matrix Metalloproteinase Stromelysin. *Biochemistry* **1992**, *31*, 10757−10762.

(25) Woessner, J. F.; Gunja-Smith, Z. Role of Metalloproteinases in Human Osteoarthritis. *J. Rheumatol.* **1991**, *18*, 99−101.

(26) Commercially available from Tripos Associates, 1699 S. Hanley Rd, Suite 303, St. Louis, MO 63144-2913. Version 6.3, operating on Silicon Graphics workstations, was used for the calculations.

(27) Commercially available from Wavefunction, Inc., 18401 Von Karman, Suite 370, Irvine, CA 92612. Version 5.1.1, operating on Silicon Graphics Octane, was used for the calculations.

(28) The IMCA-CAT facilities are supported by the companies of the Industrial Macromolecular Crystallography Association through a contract with Illinois Institute of Technology (ITT), executed through the ITT's Center for Synchrotron Radiation Research and Instrumentation. Use of the Advanced Photon Source was supported by the U.S. Department of Energy, Basic Energy Sciences, Office of Energy Research, under Contract No. W-31-109-Eng-38.

(29) Otwinowski, Z.; Minor, W. Processing of X-ray Diffraction Data Collected in Oscillation Mode. *Methods Enzymol.* **1997**, *276* (Macromolecular Crystallography, Part A), 307−326.

(30) Navaza, J. AmoRe: An Automated Package for Molecular Replacement. *Acta Crystallogr.* **1994**, *A50*, 157−163.

(31) (a) Brunger, A. T.; Kuryan, J.; Karplus, M. Crystallographic R-Factor Refinement by Molecular Dynamics. *Science* **1987**, *235*, 458−460. (b) Brunger, A. T. *X-PLOR: A System for X-ray Crystallography and NMR*; Yale University Press: New Haven, CT, 1992.

JM9903141